

Towards Accurate Human Motion Prediction via Iterative Refinement

Jiarui Sun, Girish Chowdhary
Dept. of Electrical and Computer Engineering
University of Illinois at Urbana, Champaign, USA
{jsun57, girishc}@illinois.edu

Abstract

Human motion prediction aims to forecast an upcoming pose sequence given a past human motion trajectory. To address the problem, in this work we propose FreqMRN, a human motion prediction framework that takes into account both the kinematic structure of the human body and the temporal smoothness nature of motion. Specifically, FreqMRN first generates a fixed-size motion history summary using a motion attention module, which helps avoid inaccurate motion predictions due to excessively long motion inputs. Then, supervised by the proposed spatial-temporal-aware, velocity-aware and global-smoothness-aware losses, FreqMRN iteratively refines the predicted motion through the proposed motion refinement module, which converts motion representations back and forth between pose space and frequency space. We evaluate FreqMRN on several standard benchmark datasets, including Human3.6M, AMASS and 3DPW. Experimental results demonstrate that FreqMRN outperforms previous methods by large margins for both short-term and long-term predictions, while demonstrating superior robustness.

1. Introduction

Human motion prediction aims to forecast an upcoming pose sequence given a past human motion trajectory. This task is essential for various applications, such as human tracking [34], motion generation [16], robotics [7], and autonomous driving [30]. This is a challenging task due to the large degrees of freedom of the human body, and the variability of human motion. Early data-driven methods relied on Markov models [17], Gaussian processes [36], or binary latent variables [33]. These methods capture the underlying dynamics of simple human activities, such as walking and golf swinging. However, these methods are inadequate to model more complicated motions such as playing basketball and walking a dog.

Modern methods aim to improve forecast of complicated human motion using large-scale datasets and deep learn-

ing. Among these methods, some utilize Recurrent Neural Networks (RNNs) to model temporal dynamics due to the sequential nature of human motion [6, 14, 27]. However, besides the well-known problem of training difficulty, RNN methods suffer greatly from error accumulation, which can lead to unrealistic predicted motion as the forecasting horizon increases. Recent work has shown that feed-forward methods instead can result in much better performance. Some such works use convolutional neural networks (CNNs) to learn structural and temporal correlations by treating pose sequences from human motion trajectories as regular grid structure data [3, 18]. Other works employ the attention mechanism, which enables models to capture dependencies on arbitrary structures and temporal scales [1, 24, 28]. There are also works focusing on the simplicity aspect, designing lightweight and effective models based on multi-layer perceptrons (MLPs) [2, 9]. These feed-forward approaches have not only been pushing the boundary of prediction accuracy but also greatly improve model efficiency compared to RNN-based methods.

Among feed-forward approaches, the Discrete Cosine Transform (DCT) based methods stand out due to their superior performance [5, 24, 25, 26]. Instead of learning the mapping from past motion to future motion in the pose space directly, these methods learn the differences between the padded, transformed past pose sequence and the transformed entire pose sequence in the frequency space. Specifically, they first pad the last observed pose repetitively onto the past motion trajectory until the extended input sequence has the same length as the entire motion trajectory. Then, by performing DCT on the extended input, these methods create frequency components that are very similar to those of the transformed entire pose sequence. Finally, residual learning [10] is used to make predictions. Since the frequency differences are relatively small, this technique greatly simplifies the learning problem and thus improves prediction accuracy. Another shared principle of these approaches is that they utilize Graph Convolutional Networks (GCNs) to learn the structural relationships between human body joints.

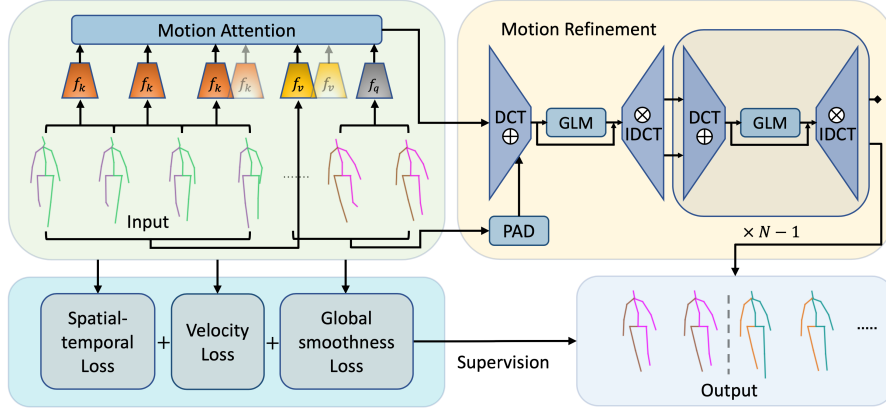


Figure 1. The proposed *FreqMRN* framework. *FreqMRN* first generates motion summary through the motion attention module, then uses the motion refinement module to predict the entire motion sequence. The model is supervised by the loss that is spatial-temporal-aware, velocity-aware and global-smoothness-aware.

In this paper, we present a framework to address some key limitations of DCT-based methods. Although these methods have greatly improved human motion prediction performance, several issues are evident. First, it was found in [25] that directly processing overly long motion history in frequency space hurts model performance because the model fails to capture small motion details, resulting in a lack of precision in the prediction. However, for complicated motions that exhibit their full characterization only over a longer period of time, a longer input motion history is necessary. Second, the last observed pose may not be the best candidate for initialization of future pose sequences [22], especially when long-term future predictions are required, where the uncertainty in motion can be large. In addition, despite being able to capture the implicit structural dependencies between joints, the GCNs used in current methods either treat all joints equally or are only aware of a simple structural hierarchy, ignoring the details of human kinematic structure.

Our main contribution to address these limitations is a framework, named *Frequency space Motion Refinement Network (FreqMRN)* for 3D human motion prediction, as illustrated in Fig. 1. *FreqMRN* first employs a motion attention module that conducts motion dependency discovery and motion aggregation for the input pose sequence at the sub-series level. Operating in pose space, the motion attention module generates a fixed-size motion history summary based on the entire input pose sequence, thus avoiding the predictor from processing too much motion information directly in the frequency space. Then, based on the latest observed motion as well as the motion history summary, a motion refinement module consisting of multiple graph learning modules is applied to gradually refine and forecast future pose sequence in a multi-stage manner. At each stage, the motion refinement module first utilizes GCNs to learn joint dependencies in the frequency space;

then, the predictions are transformed back into pose space and served as the refined input to the next graph learning module. Lastly, the predicted pose sequence is supervised by a loss that is spatial-temporal-aware, velocity-aware and global-smoothness-aware. Specifically, the loss aims to 1) take into account the degree of variation in motion in both space and time by taking into account the details of human body structure; 2) consider motion velocity and 3) consider the global smoothness of motion. This enables *FreqMRN* to capture both the spatial and temporal details of human motion and its global behavior, further regulating model predictions. During testing, *FreqMRN* generates motion trajectory of desired length in an auto-regressive manner, while incorporating information from the provided motion history as well as the previously predicted motion.

Our experiments demonstrate that *FreqMRN* outperforms previous approaches by significant margins and shows superior robustness. Specifically, we perform experiments on three standard benchmark datasets, including Human3.6M [13], AMASS [23] and 3DPW [35]. A detailed ablation study is conducted to further evaluate the benefits brought by each component of our proposed framework. We summarize our key contributions as follows:

- A novel network that iteratively refines predicted human motion by learning and converting representations back and forth between frequency space and pose space.
- A novel framework *FreqMRN* that is spatial-temporal-aware, velocity-aware and global-smoothness-aware for 3D human motion prediction, capable of emphasizing different parts of human body according to human kinematic structure.
- A comprehensive set of experiments that show the effectiveness of *FreqMRN* over state-of-the-art methods.

2. Related Work

2.1. RNN-based Methods

After the advent and rapid development of deep learning, the problem of human motion prediction is largely addressed by neural network-based methods due to their superior effectiveness. Since human motion exhibits sequential nature as time series data, RNNs are widely used to capture its temporal dynamics. Fragkiadaki *et al.* [6] proposed the ERD model, a pioneer work that augments LSTM layers [11] with encoder and decoder networks to learn the temporal dynamics and future motion representations. Jain *et al.* [14] proposed the Structural-RNN model, which incorporates spatio-temporal graphs to RNNs. Comparing to ERD, it further leverages the underlying high-level structure of human body. Instead of predicting human poses directly as in [6, 14], Martinez *et al.* [27] proposed the residual sequence-to-sequence architecture, forcing RNNs to model velocities. Recently, Li *et al.* [19] proposed the DMGNN model, which integrates graph structures to RNN units directly and models human motion in a multi-scale manner. Comparing to traditional approaches [33, 36], these methods are capable of predicting more complex motions with better performance. However, RNN-based approaches are difficult to train due to their inherent sequential nature, which also leads to issues such as severe error accumulation and prediction discontinuity.

2.2. Feed-Forward Approaches

To address the issues exhibited by RNN-based methods, attention has been turned to feed-forward approaches, which are naturally parallelizable and thus much easier to train. Some works utilize CNNs to capture both spatial and temporal correlations of human motion in a hierarchical manner [18, 20]. Although CNN-based methods are more efficient, the range of spatial and temporal correlations they capture is governed by the size of the convolutional filters, which requires laborious fine-tuning.

Starting from the seminal work of Mao *et al.* [25], the family of DCT-based approaches [4, 5, 24, 8, 25, 26] has rapidly emerged due to their promising performance. Instead of learning representations in pose space, these methods model the temporal dependence of human motion in frequency space through decoupling motion trajectories into DCT coefficients. Most of them [5, 24, 8, 25, 26] utilize GCNs for structural modeling, and the attention mechanism is used in [4, 24, 8, 26] to capture long-term temporal correlations. In particular, Mao *et al.* [26] used an ensemble of models, combining multiple DCT-based models at different scales to achieve better prediction accuracy. Guo *et al.* [8] extended the problem to the two-person situation, using a cross-attention mechanism to exploit the historical information of two interacted individuals. Dang *et al.* [5] intro-

duced the concept of hierarchy in their MSR-GCN model, while using intermediate supervision to increase model expressiveness. Ma *et al.* [22] also adopted the idea of intermediate supervision. Note that while our method and [22] both utilize multi-stage frameworks to progressively predict accurate motions, they aim to use an averaged, stage-number-based recursively smoothed target motions to guide predictions. In contrast, our approach concurrently refines the generated motion summary and query motion based on the proposed multi-component loss independent of learning stage used, and is capable of predicting human motion with any desired input-output length without sacrificing performance. Recently, MLP-based approaches [2, 9] and attention-based methods [1, 28] have been proposed, targeting at the simplicity and generalization aspects of human motion prediction frameworks.

3. Our Approach

Following previous works [24, 9], we are given human motion history $\mathbf{X}_{1:H} = \{\mathbf{x}_1, \mathbf{x}_2, \dots, \mathbf{x}_H\}$, consisting of H consecutive human poses \mathbf{x}_i . Our objective is to predict F future human poses $\mathbf{X}_{H+1:H+F} = \{\mathbf{x}_{H+1}, \mathbf{x}_{H+2}, \dots, \mathbf{x}_{H+F}\}$. Each human pose $\mathbf{x}_i \in \mathbb{R}^P$ is described by P parameters. Since we are interested in predicting 3D joint positions, $P = J \times 3$ where J denotes the number of joints.

3.1. Motion Attention Module

Since most human activities involve repetitive motion patterns, leveraging motion sub-sequence similarities in long motion history can improve prediction quality. To this end, we simply adapt the motion attention model of [24], which summarizes motion history of arbitrary length into a fixed-size representation. By aggregating the most relevant partial motions from the history, the motion attention module exploits arbitrarily long historical information while avoiding performance degradation caused by directly processing too much information in the frequency space.

In order for the motion attention module to discover motion dependencies at the sub-series level, the input motion history $\mathbf{X}_{1:H}$ is first divided into a collection of partial pose sequences $\{\mathbf{X}_{i:i+L+F-1}\}_{i=1}^{H-L-F+1}$. Each motion sub-sequence contains $L+F$ consecutive human poses, where L denotes query length and F is the length of the future motion that is to be predicted at once based on the previous L poses. The objective is to create a summarized motion representation of length $L+F$, by aggregating values $\mathbf{X}_{i:i+L+F-1}$ based on the attention scores generated from query $\mathbf{X}_{H-L+1:H}$ and keys $\mathbf{X}_{i:i+L-1}$ for all i .

To this end, the motion attention module first extract query representation and key representations. The query

$q \in \mathbb{R}^d$ and keys $k_i \in \mathbb{R}^d$ are learned as:

$$q = f_q(\mathbf{X}_{H-L+1:H}), k_i = f_k(\mathbf{X}_{i:i+L-1}), \quad (1)$$

where $f_q, f_k: \mathbb{R}^{P \times L} \rightarrow \mathbb{R}^d$ are two small CNNs mapping raw 3D motion representations to d -dimensional latent representations. Let $\mathbf{V}_i \in \mathbb{R}^{P \times (L+F)}$ denotes partial motion $\mathbf{X}_{i:i+L+F-1}$. Then, the attention scores and motion summary $\mathbf{S} \in \mathbb{R}^{P \times (L+F)}$ are computed as:

$$a_i = \frac{qk_i^T}{\sum_{j=1}^{H-L-F+1} qk_j^T}, \mathbf{S} = \sum_{i=1}^{H-L-F+1} a_i \mathbf{V}_i, \quad (2)$$

such that $\sum_i a_i = 1$. ReLU is used [29] as the output layer for f_q and f_k to avoid negative a_i .

While being conceptually the same, the empirical differences between the original motion attention model and ours is that instead of using values \mathbf{V}_i in the frequency space as in [24], our motion attention module operates only in pose space, reducing computational overhead. More importantly, the motion summary \mathbf{S} is used together with the query $\mathbf{X}_{H-L+1:H}$ as an auxiliary input to the motion refinement module to guide the refinement process. During testing, if we want to generate longer future motion, the motion attention module is capable of incorporating new predictions by iteratively augmenting the motion history with new predictions as input. As such, the motion attention module can utilize history information of arbitrary length, while avoiding generating excessively long motions that may impair model performance.

3.2. Motion Refinement Module

The motion refinement module aims to predict future motion based on the latest observed motion $\mathbf{X}_{H-L+1:H}$ and the motion summary \mathbf{S} generated from the motion attention module. The core of this module is to iteratively refine the predicted human motion by converting representations back and forth between the original 3D pose space and the DCT space. Specifically, the module consists of two components: the domain conversion unit and the graph learning module. We present both of them as follows.

Domain conversion unit. Among DCT-based human motion prediction methods, most prior works [24, 25, 26] aim to learn the differences between the padded, transformed past pose sequence and the transformed entire pose sequence in the DCT space. Specifically, for a motion history of length L , these approaches first convert the original input pose sequence to $\mathbf{X}'_0 \in \mathbb{R}^{P \times (L+F)}$ in DCT space as:

$$\mathbf{X}_0 = [\mathbf{X}_{H-L+1:H}; \mathbf{X}_H \times F], \mathbf{X}'_0 = \mathcal{D}(\mathbf{X}_0), \quad (3)$$

where $\mathcal{D}(\cdot)$ denotes the DCT operation. Then, the output pose sequence $\mathbf{X}_N \in \mathbb{R}^{P \times (L+F)}$ is generated as:

$$\mathbf{X}_N = \mathcal{D}^{-1}(\mathcal{F}(\mathbf{X}'_0) + \mathbf{X}'_0), \quad (4)$$

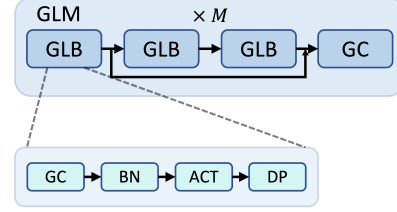


Figure 2. The proposed graph learning module. It consists of multiple graph learning blocks with residual connections.

where $\mathcal{D}^{-1}(\cdot)$ denotes the inverse DCT (IDCT) operation, $\mathcal{F}(\cdot)$ is the residual predictor, and N represents the number of learning stages. The last F poses of \mathbf{X}_N are evaluated against groundtruth $\mathbf{X}_{H+1:H+F}$ for model performance.

From the above learning pipeline, it is clear that the learning difficulty is closely related to the actual differences between \mathbf{X}_0 and $\mathbf{X}_{H-L+1:H+F}$ [5, 22]. In extreme cases, the learning problem becomes trivial if the person stops moving at the prediction horizon. Inspired by this observation, instead of learning the future motion all at once, we learn to iteratively refine the predicted motion through converting representations back and forth between pose space and DCT space via domain conversion units. Recall that N denotes the number of iterations. Now, after Eq. (3), \mathbf{X}_N can be computed iteratively as:

$$\mathbf{X}_n = \mathcal{D}^{-1}(\mathcal{F}_n(\mathbf{X}'_{n-1}) + \mathbf{X}'_{n-1}), \mathbf{X}'_n = \mathcal{D}(\mathbf{X}_n), \quad (5)$$

where $\mathcal{F}_n(\cdot)$ is the n^{th} residual predictor.

However, the above predictor only exploits the L latest poses, as directly considering the entire H past poses is detrimental to performance [25]. To this end, we propose to integrate the motion summary \mathbf{S} from the motion attention module to Eq. (5). Let $\mathbf{S}_0 = \mathbf{S}$. The motion refinement module predicts motion as:

$$\mathbf{G}'_{n-1} = [\mathcal{D}(\mathbf{S}_{n-1}); \mathcal{D}(\mathbf{X}_{n-1})], \quad (6)$$

$$[\mathbf{S}'_n; \mathbf{X}'_n] = \mathcal{F}_n(\mathbf{G}'_{n-1}) + \mathbf{G}'_{n-1}, \quad (7)$$

$$\mathbf{S}_n = \mathcal{D}^{-1}(\mathbf{S}'_n), \mathbf{X}_n = \mathcal{D}^{-1}(\mathbf{X}'_n), \quad (8)$$

where $\mathbf{G}'_{n-1} \in \mathbb{R}^{P \times 2(L+F)}$ represents the concatenation of the motion summary and the predicted motion representation. At the N^{th} stage, \mathbf{S}_N is discarded.

Graph learning module. The residual predictor, *i.e.*, the graph learning module (GLM) $\mathcal{F}_n(\cdot)$ aims to capture structural and temporal dependencies across human joints and DCT components. The architecture is shown in Fig. 2. It contains K graph learning blocks (GLBs), each of which is based on the graph convolution (GC) operation. At the k^{th} block, the GC operation is defined as:

$$\text{GC}(\mathbf{G}') = \mathbf{A}_k \mathbf{G}' \mathbf{W}_k, \quad (9)$$

where $\mathbf{A}_k \in \mathbb{R}^{P \times P}$ defines the learnable structural graph adjacency matrix and $\mathbf{W}_k \in \mathbb{R}^{d \times d'}$ denotes the weight matrix for temporal modeling at the k^{th} layer.

Based on the GC operation, each GLB sequentially executes GC, batch normalization [12], tanh activation and dropout [32]. Let $\mathbf{G}'_0 \in \mathbb{R}^{P \times 2(L+F)}$ denotes the input. As shown in Fig. 2, we define the GLM $\mathcal{F}(\cdot)$ as:

$$\mathbf{G}'_1 = \text{GLB}_1(\mathbf{G}'_0), \quad (10)$$

$$\mathbf{G}'_{k+2} = \text{GLB}_{k+2}(\text{GLB}_{k+1}(\mathbf{G}'_k)) + \mathbf{G}'_k, \quad (11)$$

$$\mathbf{G}'_{\text{out}} = \text{GC}(\mathbf{G}'_K), \quad (12)$$

where $k = 1, 3, \dots, K$ denotes GLB iteration index. The last GC operation is used to ensure $\mathbf{G}'_{\text{out}} \in \mathbb{R}^{P \times 2(L+F)}$, that it has the correct number of DCT components for frequency-pose conversion.

3.3. Learning Algorithm

Using the proposed motion attention module and motion refinement module, we predict 3D human poses in an end-to-end manner. During training, most prior works [24, 9, 25] considers the ℓ_2 loss as supervision. However, the ℓ_2 loss simply treats all joints equally, ignoring this important kinematic structure of the human body. In addition, it also treats all poses equally across time, which leaves the error accumulation issue unaddressed. Although such issue is not as severe as for RNNs, predicting accurate initial poses can still help predict later poses, especially for multi-stage networks. To this end, we propose the following losses that help regulate the model to obtain accurate predictions.

Spatial-temporal-aware loss. To account for variations in the spatial and temporal aspects of human motion, we propose to weight the joint representations differently as:

$$\mathcal{L}_{st} = \frac{1}{J(L+F)} \sum_{f=1}^{L+F} \sum_{j=1}^J \|(\mathbf{X}_j^f - \tilde{\mathbf{X}}_j^f) \cdot \lambda_j^f\|_2, \quad (13)$$

$$\sum_{f=1}^{L+F} \sum_{j=1}^J \lambda_j^f = J(L+F), \quad (14)$$

where \mathbf{X}_j^f and $\tilde{\mathbf{X}}_j^f$ are the groundtruth and predicted representations of the j^{th} joint at the f^{th} frame respectively, and λ_j^f denotes the specific assigned weight. The weights are computed based on the specifics of the kinematic structure and their temporal index, and they do not require learning.

Specifically, let $\mathbf{X} = \{\mathbf{x}_1, \mathbf{x}_2, \dots, \mathbf{x}_F\}$ denotes predicted motion, where $\mathbf{x} \in \mathbb{R}^{J \times 3}$ describes the 3D coordinates of one particular human pose. Based on the kinematic structure of the human body, each pose \mathbf{x} can be described by \mathcal{L} kinematic chains. Let c_l denote the l^{th} kinematic chain, b_l^i denote the bone length of the i^{th} bone on

c_l , and $l(c_l)$ denote the total number of bones of c_l . Form the spatial perspective, suppose that the j^{th} joint is the j^{th} joint on chain c_l . We define:

$$\lambda_j^f \propto \frac{j'}{l(c_l)} \ln \left(\sum_{i'=1}^{j'} b_{i'} \right). \quad (15)$$

From the temporal perspective, suppose that the f^{th} joint is the f^{th} joint enumerating from the prediction horizon. We define:

$$\lambda_j^f \propto (F - f + L) \quad \text{if } f > L, \quad (16)$$

$$\lambda_j^f \propto (1) \quad \text{otherwise.} \quad (17)$$

In particular, from the structural point of view, higher weights are assigned to joints that may exhibit vigorous motions (external joints). From the temporal perspective, higher weights are assigned to joints that are closer to the prediction horizon.

Velocity-aware loss. Since most human motions tend to be smooth, following [9], we adopt the velocity-aware loss to further regulate the predicted motion trajectories. It is computed as:

$$\mathcal{L}_v = \frac{1}{J(L+F-1)} \sum_{f=1}^{L+F-1} \sum_{j=1}^J \|(\mathbf{V}_j^f - \tilde{\mathbf{V}}_j^f)\|_2, \quad (18)$$

where \mathbf{V}_j^f and $\tilde{\mathbf{V}}_j^f$ are the groundtruth and predicted joint velocities, computed as joint displacements between consecutive frames.

Global-smoothness-aware loss. Note that for both proposed losses, instead of only focusing on the unobserved future motion of length F , we also aim to reconstruct the last observed L poses. Through reconstructing the query motion, *FreqMRN* is aware of the entire pose trajectory in a global sense thus further regulate its prediction. The learning algorithm aims to optimize the overall loss, which is defined as:

$$\mathcal{L} = \mathcal{L}_{st} + \mathcal{L}_v. \quad (19)$$

We provide detailed ablation analysis for the loss choices in Sec. 4.4.

4. Experiments

In this section, we evaluate the effectiveness of *FreqMRN*. We first present the datasets we used in Sec. 4.1. Then, we introduce our experimental setup in Sec. 4.2, including evaluation metrics, baseline methods for comparison and model implementation details. The quantitative and qualitative results are presented in Sec. 4.3. A detailed ablation analysis is performed and presented in Sec. 4.4 to evaluate the effectiveness of the proposed framework.

scenarios	walking				eating				smoking				discussion			
	80ms	400ms	560ms	1000ms	80ms	400ms	560ms	1000ms	80ms	400ms	560ms	1000ms	80ms	400ms	560ms	1000ms
ResSup [27]	23.2	66.1	71.6	79.1	16.8	61.7	74.9	98.0	18.9	65.4	78.1	102.1	25.7	91.3	109.5	131.8
convSeq2Seq [18]	17.7	63.6	72.2	82.3	11.0	48.4	61.3	87.1	11.6	48.9	60.0	81.7	17.1	77.6	98.1	129.3
LTD-50-25 [25]	12.3	44.4	50.7	60.3	7.8	38.6	51.5	75.8	8.2	39.5	50.5	72.1	11.9	68.1	88.9	118.5
LTD-10-10 [25]	11.1	42.9	53.1	70.7	7.0	37.3	51.1	78.6	7.5	37.5	49.4	71.8	10.8	65.8	88.1	121.6
HRI [24]	10.0	39.8	47.4	58.1	6.4	36.2	50.0	75.7	7.0	36.4	47.6	69.5	10.2	65.4	86.6	119.8
STDGCN [22]	11.2	42.8	49.6	58.9	6.5	36.8	50.0	74.9	7.3	37.5	48.8	69.9	10.2	64.4	86.1	116.9
MMA [26]	9.9	39.0	46.2	57.1	6.2	35.3	48.6	73.7	6.8	35.5	46.5	68.7	9.9	64.0	85.2	117.5
siMLPe [9]	9.9	39.6	46.8	55.7	5.9	36.1	49.6	74.5	<u>6.5</u>	36.3	47.2	69.3	<u>9.4</u>	64.3	85.7	116.3
Ours	9.0	36.7	44.5	54.1	5.6	33.9	47.2	73.1	6.2	35.1	46.9	<u>69.2</u>	8.7	62.9	84.7	117.1
scenarios	directions				greeting				phoning				posing			
	80ms	400ms	560ms	1000ms	80ms	400ms	560ms	1000ms	80ms	400ms	560ms	1000ms	80ms	400ms	560ms	1000ms
ResSup [27]	21.6	84.1	101.1	129.1	31.2	108.8	126.1	153.9	21.1	76.4	94.0	126.4	29.3	114.3	140.3	183.2
convSeq2Seq [18]	13.5	69.7	86.6	115.8	22.0	96.0	116.9	147.3	13.5	59.9	77.1	114.0	16.9	92.9	122.5	187.4
LTD-50-25 [25]	8.8	58.0	74.2	105.5	16.2	82.6	104.8	136.8	9.8	50.8	68.8	105.1	12.2	79.9	110.2	174.8
LTD-10-10 [25]	8.0	54.9	76.1	108.8	14.8	79.7	104.3	140.2	9.3	49.7	68.7	105.1	10.9	75.9	109.9	171.7
HRI [24]	7.4	56.5	73.9	106.5	13.7	78.1	101.9	138.8	8.6	49.2	67.4	105.0	10.2	75.8	107.6	178.2
STDGCN [22]	7.5	56.0	73.3	105.9	14.0	77.3	100.2	136.4	8.7	48.8	66.5	102.7	10.2	73.3	102.8	167.0
MMA [26]	7.2	<u>55.0</u>	<u>72.4</u>	<u>105.7</u>	13.6	<u>77.2</u>	100.5	136.7	8.4	<u>48.4</u>	66.5	104.6	9.8	74.9	105.8	172.9
siMLPe [9]	6.5	55.8	73.1	106.7	<u>12.4</u>	77.3	99.8	137.5	<u>8.1</u>	48.6	66.3	103.3	<u>8.8</u>	73.8	103.4	168.7
Ours	6.3	52.8	69.8	104.4	11.6	72.8	97.7	<u>136.5</u>	7.6	46.5	64.6	<u>103.3</u>	8.3	70.7	101.0	166.4
scenarios	purchases				sitting				sitting down				taking photo			
	80ms	400ms	560ms	1000ms	80ms	400ms	560ms	1000ms	80ms	400ms	560ms	1000ms	80ms	400ms	560ms	1000ms
ResSup [27]	28.7	100.7	122.1	154.0	23.8	91.2	113.7	152.6	31.7	112.0	138.8	187.4	21.9	87.6	110.6	153.9
convSeq2Seq [18]	20.3	89.9	111.3	151.5	13.5	63.1	82.4	120.7	20.7	82.7	106.5	150.3	12.7	63.6	84.4	128.1
LTD-50-25 [25]	15.2	78.1	99.2	134.9	10.4	58.3	79.2	118.7	17.1	76.4	100.2	143.8	9.6	54.3	75.3	118.8
LTD-10-10 [25]	13.9	75.9	99.4	135.9	9.8	55.9	78.5	118.8	15.6	71.7	96.2	142.2	8.9	51.7	72.5	116.3
HRI [24]	13.0	73.9	95.6	134.2	9.3	56.0	76.4	115.9	14.9	72.0	97.0	143.6	8.3	51.5	72.1	115.9
STDGCN [22]	13.2	74.0	95.7	132.1	9.1	<u>54.6</u>	<u>75.1</u>	114.8	14.7	70.0	94.4	139.0	8.2	50.2	<u>70.5</u>	112.9
MMA [26]	12.8	72.8	94.5	133.1	9.1	55.4	75.8	115.0	14.7	71.3	96.0	141.8	8.2	51.1	71.8	115.2
siMLPe [9]	11.7	72.4	93.8	132.5	8.6	55.2	75.4	114.1	13.6	70.8	95.7	142.4	7.8	50.8	71.0	112.8
Ours	11.1	71.7	93.0	132.7	8.4	53.8	74.7	<u>114.5</u>	13.5	<u>70.4</u>	<u>95.1</u>	<u>141.6</u>	7.5	49.1	69.5	111.6
scenarios	waiting				walking dog				walking together				average			
	80ms	400ms	560ms	1000ms	80ms	400ms	560ms	1000ms	80ms	400ms	560ms	1000ms	80ms	400ms	560ms	1000ms
ResSup [27]	23.8	87.7	105.4	135.4	36.4	110.6	128.7	164.5	20.4	67.3	80.2	98.2	25.0	88.3	106.3	136.6
convSeq2Seq [18]	14.6	68.7	87.3	117.7	27.7	103.3	122.4	162.4	15.3	61.2	72.0	87.4	16.6	72.7	90.7	124.2
LTD-50-25 [25]	10.4	59.2	77.2	108.3	22.8	88.7	107.8	156.4	10.3	46.3	56.0	65.7	12.2	61.5	79.6	112.4
LTD-10-10 [25]	9.2	54.4	73.4	107.5	20.9	86.6	109.7	150.1	9.6	44.0	55.7	69.8	11.2	58.9	78.3	114.0
HRI [24]	8.7	54.9	74.5	108.2	20.1	86.3	108.2	146.9	8.9	41.9	52.7	64.9	10.4	58.3	77.3	112.1
STDGCN [22]	8.7	53.6	71.6	<u>103.7</u>	20.4	84.6	105.7	145.9	8.9	43.8	54.4	64.6	10.6	57.9	76.3	109.7
MMA [26]	8.4	53.8	72.7	105.1	19.6	<u>84.1</u>	105.1	<u>141.4</u>	8.5	<u>41.1</u>	51.2	63.2	10.2	57.3	75.9	110.1
siMLPe [9]	7.8	53.2	71.6	104.6	18.2	83.6	105.6	141.2	8.4	41.2	50.8	61.5	9.6	57.3	75.7	<u>109.4</u>
Ours	7.2	50.5	69.0	103.4	17.8	87.0	112.0	147.5	7.7	38.5	48.5	<u>61.9</u>	9.1	55.5	74.5	109.2

Table 1. Action-wise prediction results on Human3.6M dataset. MPJPE in millimeter at particular frames are reported. 256 samples are tested for each action. The best results are highlighted in **bold**, and the second best results are underlined.

4.1. Datasets

Human3.6M [13] is the most widely used benchmark dataset for human motion prediction. It contains 15 distinct actions performed by 7 subjects, and each human pose contains 32 joints in exponential map format. Following [25], 3D coordinates of the joints are computed based on forward kinematics of the skeleton, and 10 redundant joints are removed. For a fair comparison with [24, 25], we use subject 11 and subject 5 for validation and testing, and the rest for training.

AMASS [23] unifies multiple Mocap datasets, such as the popular CMU-MoCap dataset using a shared SMPL [21] parameterization. As in the Human3.6M case, 3D coordinates are obtained and 18 joints are used following [24]. Other settings including frame-rate, train/validate/test partition and testing protocol are all adjusted to be the same as previous works [24, 26] for fair comparisons.

3DPW [35] consists of actions performed in challenging scenes. Following [24], we only evaluate our model trained on the AMASS dataset on the test partition of 3DPW, aiming to examine the generalization of our method. All settings are adjusted to be the same as [24].

4.2. Experimental Setup

Evaluation metrics. We use the *Mean Per Joint Position Error* (MPJPE) for performance evaluation, which is the most widely used evaluation metric for 3D human motion prediction. Specifically, MPJPE calculates the averaged ℓ_2 difference between the predicted pose sequence and the corresponding groundtruth across all joints. As in previous works [24, 25], we report MPJPE at individual frames.

Baselines. We compare our model performance with one RNN-based method, ResSup [27], one CNN-based method convSeq2Seq [18], and multiple feed-forward methods, including LTD [25], HRI [24], STDGCN [22], MMA [26] and siMLPe [9], constituting the state of the art. The results of MMA are taken from [26], and all other results are taken from [9]. Note that LTD results are based on different configurations: the numbers indicate observed frames and predicted frames respectively during training.

Implementation details. We use PyTorch [31] to implement *FreqMRN*. We set input length $H = 50$, query length $L = 10$ and output length $F = 10$ for Human3.6M and $F = 25$ for AMASS and 3DPW datasets following prior works [24, 9] for fair comparisons.

dataset	AMASS								3DPW							
	80ms	160ms	320ms	400ms	560ms	720ms	880ms	1000ms	80ms	160ms	320ms	400ms	560ms	720ms	880ms	1000ms
milliseconds																
convSeq2Seq [18]	20.6	36.9	59.7	67.6	79.0	87.0	91.5	93.5	18.8	32.9	52.0	58.8	69.4	77.0	83.6	87.8
LTD-10-10 [25]	<u>10.3</u>	<u>19.3</u>	36.6	44.6	61.5	75.9	86.2	91.2	<u>12.0</u>	<u>22.0</u>	38.9	46.2	59.1	69.1	76.5	81.1
LTD-10-25 [25]	11.0	20.7	37.8	45.3	57.2	65.7	71.3	75.2	12.6	23.2	39.7	46.6	57.9	65.8	71.5	75.5
HRI [24]	11.3	20.7	35.7	42.0	51.7	58.6	63.4	67.2	12.6	23.1	39.0	45.4	56.0	63.6	69.7	73.7
MMA [26]	11.0	20.3	35.0	41.2	50.7	57.4	61.9	65.8	12.4	22.6	38.1	44.4	54.7	62.1	67.9	71.8
siMLPe [9]	10.8	19.6	34.3	40.5	50.5	57.3	62.4	65.7	12.1	22.1	38.1	44.5	54.9	62.4	68.2	72.2
Ours	9.8	17.8	31.8	37.9	47.8	55.3	60.7	65.4	11.6	20.8	36.4	42.8	53.3	61.0	66.9	71.0

Table 2. Short-term and long-term prediction results on AMASS and 3DPW datasets. The models are trained on the AMASS dataset. MPJPE in millimeter at particular frames are reported. The best results are highlighted in **bold**, and the second best results are underlined.

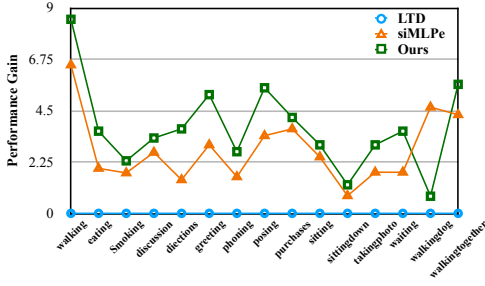


Figure 3. Action-wise performance gains for Human3.6M.

For the motion attention module, $f_q(\cdot)$ and $f_k(\cdot)$ are implemented as 2-layer CNNs. For the motion refinement module, we iteratively perform $N = 3$ learning stages, each of which contains $K = 5$ GLBs ($M = 2$) with dropout ratio 0.3. We set $d = 256$ as latent representation dimension across different components of *FreqMRN*.

Adam [15] is used as the optimizer for all experiments, with 0.005 as the initial learning rate. For Human3.6M dataset, the model is trained for 200 epochs with 32 as the batch size, and the learning rate is multiplied by 0.97 at each epoch. For AMASS and 3DPW datasets, we train the model for 250 epochs with batch size 128, and the learning rate is multiplied by 0.98 at each epoch. We use NVIDIA V100 GPUs for all experiments. For more model implementation details, please refer to the supplementary material.

4.3. Results

In this section, we compare *FreqMRN* with the selected baselines on various datasets. We report the MPJPE evaluated at specific frames in millimeters as in [24, 9].

Human3.6M. For Human3.6M, we quantitatively report the performance comparison for short-term prediction and long-term prediction in Tab. 1. Tables with more details are provided in the supplementary material. *FreqMRN* outperforms selected baselines on average for both short-term and long-term prediction by significant margins. In Fig. 3, we also show the action-wise performance gain for *FreqMRN* and siMLPe with respect to LTD. We can observe that our method demonstrates large performance gains for actions with repetitive patterns such as “eating”, taking advantages of the motion summary generated by the motion attention module. However, we interestingly note that our

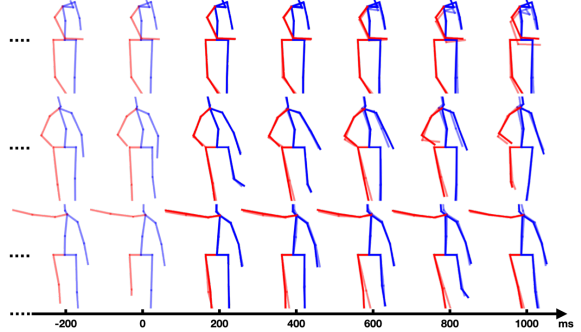


Figure 4. Qualitative comparisons with groundtruth for “sitting” (top), “walking” (middle) and “walkingtogether” (bottom) actions from Human3.6M. Solid lines represent predictions, and transparent lines represent groundtruth.

method does not perform as well on the “walkingdog” action as other actions. We believe this is due to the inherently large periodicity of this particular action, resulting in the current motion summary not helping the model to make better predictions. We validate our hypothesis in the last part of the ablation study.

In terms of qualitative evaluation, in Fig. 4, we show the visualized predicted motion with respect to the correspond groundtruth motion for action “eating”, “walking” and “walkingdog” of Human3.6M. We can see that the predictions generated from *FreqMRN* match the groundtruth motion consistently in both shot-term and long-term.

AMASS and 3DPW. For AMASS and 3DPW, we report performance comparisons quantitatively at particular frames in Tab. 2. As previously mentioned, the model is trained on the AMASS dataset and tested on the test partition of AMASS and 3DPW separately as in [24, 9]. In both experiments, *FreqMRN* consistently outperforms selected baselines across all evaluated frames by large margins. The superior performance on 3DPW further demonstrates the robustness of our proposed method.

4.4. Ablation Analysis

In this section, We conduct an ablation study on Human3.6M dataset to investigate how different components of *FreqMRN* may affect its motion modeling ability.

Model architecture. We first show how each design choice

variant	80ms	400ms	560ms	1000ms	average
single stage, no attention, no loss guidance	21.3	79.9	104.6	143.1	87.2
no motion attention guidance	18.9	78.6	101.8	139.1	84.6
without iterative refinement	9.8	56.4	75.3	110.1	62.9
without multi-component loss	9.7	56.4	75.5	109.8	62.9
full model	9.1	55.5	74.5	109.2	62.1

Table 3. Ablation on *FreqMRN*'s architecture.

N-M	80ms	160ms	320ms	400ms	560ms	720ms	880ms	1000ms
1-6	9.8	21.7	45.5	56.4	75.3	90.0	102.2	110.1
2-3	9.3	21.1	45.0	55.8	74.8	89.5	101.6	109.5
6-1	9.1	20.7	44.6	55.7	74.9	89.6	101.7	109.5
4-2	9.1	20.8	44.9	56.0	75.1	89.8	101.9	109.9
5-2	9.0	20.7	44.8	55.8	74.9	89.7	101.8	109.7
6-2	8.9	20.7	44.9	55.9	74.9	89.5	101.5	109.4
3-2 (ours)	9.1	20.7	44.5	55.5	74.5	89.2	101.3	109.2

Table 4. Ablation on learning stage configurations.

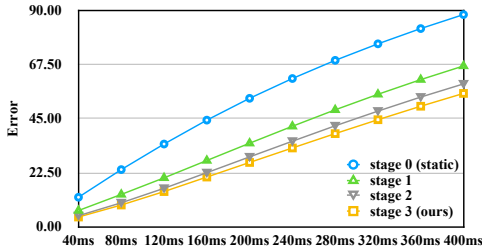


Figure 5. Frame-wise error across different refinement stages: 0 (static) to 4 (ours) for Human3.6M.

improves the effectiveness of *FreqMRN*, including 1) the motion attention module 2) the multi-stage motion refinement module, and 3) the multi-component loss. All ablation results are shown in Tab. 3. Recall that the full model has $N = 3$ refining stages each containing $M = 2$ GLM stages, denoting as 3-2 configuration. The averaged prediction error is 62.1. We first establish a plain baseline model which does not utilize the proposed attention module, refinement module and multi-component loss. The prediction error drastically rises to 87.23. 1) To validate the effectiveness of motion attention guidance, we replace the motion attention module with the ‘‘Copy’’ operator [22] in the full model, leading to a large prediction error of 84.61. 2) Instead of using 3-2 configuration, we use 1-6 configuration, corresponding to a single-stage model with similar computational power. The prediction error becomes 62.9. 3) Lastly, we use the simple ℓ_2 loss to supervise *FreqMRN*, also yielding a 62.9 prediction error.

Number of learning stages. In Tab. 4, we study the specific configuration of the motion refinement module. We first examine configurations with similar computational power, and then gradually increase the number of refinements performed while keeping the number of GLMs used per refinement stage fixed. As shown in the table, *FreqMRN* achieves the best performance with the 3-2 configuration.

Loss components. In Tab. 5, we conduct a detailed ablation study on the proposed loss components. From the table, we observe that all components help *FreqMRN* achieve

variant	80ms	160ms	320ms	400ms	560ms	720ms	880ms	1000ms
w/o s.t. weights	9.4	21.2	45.3	56.2	75.1	89.7	101.7	109.4
w/o \mathcal{L}_v	9.1	20.7	44.6	55.7	75.1	89.8	101.9	109.7
w/o query reconst.	9.2	20.9	44.9	55.8	74.8	89.5	101.8	109.7
$\mathcal{L}_{st} + \mathcal{L}_v$ (ours)	9.1	20.7	44.5	55.5	74.5	89.2	101.3	109.2

Table 5. Ablation on loss configurations.

variant	80ms	160ms	320ms	400ms	560ms	720ms	880ms	1000ms
ours-50	17.8	37.9	72.8	87.0	112.0	124.2	137.7	147.5
ours-100	17.7	38.0	73.5	87.4	111.5	121.9	134.8	145.1

Table 6. Results on feeding selected sequences: ‘‘walkingdog’’ action that contain similar patterns in longer history. Number indicates observed frames during testing.

better performance across all frames, while each component has its own focus. In particular, the spatial-temporal-aware loss puts more emphasis on short-term prediction, while the velocity-aware loss focuses more on long-term improvement. Besides, the global-smoothness-aware loss uniformly improves the global performance. It is evident that the proposed loss is indispensable to *FreqMRN*, especially the spatial-temporal-aware loss that considers human kinematic structure.

Benefit of refinement. To further validate and demonstrate the effectiveness of the motion refinement module, we show the frame-wise error of motion generated from each stage of refinement, *i.e.*, stage-wise model outputs from $N = 0$ to $N = 3$ with respect to the groundtruth in Fig. 5. We can observe that the error decreases steadily at each stage. This indicates that the motion refinement module successfully predicts better motion as it iteratively generates refined motion that is closer to the groundtruth, greatly reducing the learning difficulty.

Arbitrary length history handling. To demonstrate *FreqMRN*'s ability of handling inputs of arbitrary length, we show the results of feeding different numbers of observed frames of into to *FreqMRN* during testing in Tab. 6. From the table, we can see that the benefits of using longer history motion becomes more evident in long prediction horizon.

5. Conclusion

In this work, we present *FreqMRN*, a novel framework for human motion prediction. Specifically, we propose 1) a motion attention module that generates motion summary, and 2) a motion refinement module that predicts future motion in a multi-stage manner using the latest observed motion and motion summary. We also propose 3) a multi-component loss which is spatial-temporal-aware, velocity-aware and global-smoothness-aware, guiding the model to predict realistic motion in both short-term and long-term. The results obtained from extensive experiments and detailed analysis show that *FreqMRN* has significant performance gains over state-of-the-art baselines on benchmark datasets, demonstrating the effectiveness of our method.

References

- [1] Emre Aksan, Manuel Kaufmann, Peng Cao, and Otmar Hilliges. A spatio-temporal transformer for 3d human motion prediction. In *International Conference on 3D Vision, 3DV 2021, London, United Kingdom, December 1-3, 2021*, pages 565–574, 2021. [1](#), [3](#)
- [2] Arij Bouazizi, Adrian Holzbock, Ulrich Kressel, Klaus Dietmayer, and Vasileios Belagiannis. Motionmixer: Mlp-based 3d human body pose forecasting. In *Proceedings of the Thirty-First International Joint Conference on Artificial Intelligence, IJCAI 2022, Vienna, Austria, 23-29 July 2022*, pages 791–798, 2022. [1](#), [3](#)
- [3] Judith Bütetage, Michael J. Black, Danica Kragic, and Hedvig Kjellström. Deep representation learning for human motion prediction and classification. In *2017 IEEE Conference on Computer Vision and Pattern Recognition, CVPR 2017, Honolulu, HI, USA, July 21-26, 2017*, pages 1591–1599, 2017. [1](#)
- [4] Yujun Cai, Lin Huang, Yiwei Wang, Tat-Jen Cham, Jianfei Cai, Junsong Yuan, Jun Liu, Xu Yang, Yiheng Zhu, Xiaohui Shen, Ding Liu, Jing Liu, and Nadia Magnenat-Thalmann. Learning progressive joint propagation for human motion prediction. In *Computer Vision - ECCV 2020 - 16th European Conference, Glasgow, UK, August 23-28, 2020, Proceedings, Part VII*, pages 226–242, 2020. [3](#)
- [5] Lingwei Dang, Yongwei Nie, Chengjiang Long, Qing Zhang, and Guiqing Li. MSR-GCN: multi-scale residual graph convolution networks for human motion prediction. In *2021 IEEE/CVF International Conference on Computer Vision, ICCV 2021, Montreal, QC, Canada, October 10-17, 2021*, pages 11447–11456, 2021. [1](#), [3](#), [4](#)
- [6] Katerina Fragkiadaki, Sergey Levine, Panna Felsen, and Jitendra Malik. Recurrent network models for human dynamics. In *2015 IEEE International Conference on Computer Vision, ICCV 2015, Santiago, Chile, December 7-13, 2015*, pages 4346–4354, 2015. [1](#), [3](#)
- [7] Liang-Yan Gui, Kevin Zhang, Yu-Xiong Wang, Xiaodan Liang, José M. F. Moura, and Manuela Veloso. Teaching robots to predict human motion. In *2018 IEEE/RSJ International Conference on Intelligent Robots and Systems, IROS 2018, Madrid, Spain, October 1-5, 2018*, pages 562–567, 2018. [1](#)
- [8] Wen Guo, Xiaoyu Bie, Xavier Alameda-Pineda, and Francesc Moreno-Noguer. Multi-person extreme motion prediction. In *IEEE/CVF Conference on Computer Vision and Pattern Recognition, CVPR 2022, New Orleans, LA, USA, June 18-24, 2022*, pages 13043–13054, 2022. [3](#)
- [9] Wen Guo, Yuming Du, Xi Shen, Vincent Lepetit, Xavier Alameda-Pineda, and Francesc Moreno-Noguer. Back to MLP: A simple baseline for human motion prediction. In *IEEE/CVF Winter Conference on Applications of Computer Vision, WACV 2023, Waikoloa, HI, USA, January 2-7, 2023*, pages 4798–4808, 2023. [1](#), [3](#), [5](#), [6](#), [7](#), [12](#)
- [10] Kaiming He, Xiangyu Zhang, Shaoqing Ren, and Jian Sun. Deep residual learning for image recognition. In *2016 IEEE Conference on Computer Vision and Pattern Recognition, CVPR 2016, Las Vegas, NV, USA, June 27-30, 2016*, pages 770–778, 2016. [1](#)
- [11] Sepp Hochreiter and Jürgen Schmidhuber. Long short-term memory. *Neural Comput.*, 9(8):1735–1780, 1997. [3](#)
- [12] Sergey Ioffe and Christian Szegedy. Batch normalization: Accelerating deep network training by reducing internal covariate shift. In *Proceedings of the 32nd International Conference on Machine Learning, ICML 2015, Lille, France, 6-11 July 2015*, pages 448–456, 2015. [5](#), [11](#)
- [13] Catalin Ionescu, Dragos Papava, Vlad Olaru, and Cristian Sminchisescu. Human3.6m: Large scale datasets and predictive methods for 3d human sensing in natural environments. *IEEE Trans. Pattern Anal. Mach. Intell.*, 36(7):1325–1339, 2014. [2](#), [6](#)
- [14] Ashesh Jain, Amir R. Zamir, Silvio Savarese, and Ashutosh Saxena. Structural-rnn: Deep learning on spatio-temporal graphs. In *2016 IEEE Conference on Computer Vision and Pattern Recognition, CVPR 2016, Las Vegas, NV, USA, June 27-30, 2016*, pages 5308–5317, 2016. [1](#), [3](#)
- [15] Diederik P. Kingma and Jimmy Ba. Adam: A method for stochastic optimization. In *ICLR*, 2015. [7](#), [11](#)
- [16] Lucas Kovar, Michael Gleicher, and Frédéric H. Pighin. Motion graphs. *ACM Trans. Graph.*, 21(3):473–482, 2002. [1](#)
- [17] Andreas M. Lehrmann, Peter V. Gehler, and Sebastian Nowozin. Efficient nonlinear markov models for human motion. In *2014 IEEE Conference on Computer Vision and Pattern Recognition, CVPR 2014, Columbus, OH, USA, June 23-28, 2014*, pages 1314–1321. IEEE Computer Society, 2014. [1](#)
- [18] Chen Li, Zhen Zhang, Wee Sun Lee, and Gim Hee Lee. Convolutional sequence to sequence model for human dynamics. In *2018 IEEE Conference on Computer Vision and Pattern Recognition, CVPR 2018, Salt Lake City, UT, USA, June 18-22, 2018*, pages 5226–5234, 2018. [1](#), [3](#), [6](#), [7](#), [12](#)
- [19] Maosen Li, Siheng Chen, Yangheng Zhao, Ya Zhang, Yanfeng Wang, and Qi Tian. Dynamic multiscale graph neural networks for 3d skeleton based human motion prediction. In *2020 IEEE/CVF Conference on Computer Vision and Pattern Recognition, CVPR 2020, Seattle, WA, USA, June 13-19, 2020*, pages 211–220, 2020. [3](#)
- [20] Xiaoli Liu, Jianqin Yin, Jin Li, Pengxiang Ding, Jun Liu, and Huaping Liu. Trajectorycnn: A new spatio-temporal feature learning network for human motion prediction. *IEEE Trans. Circuits Syst. Video Technol.*, 31(6):2133–2146, 2021. [3](#)
- [21] Matthew Loper, Naureen Mahmood, Javier Romero, Gerard Pons-Moll, and Michael J. Black. SMPL: a skinned multi-person linear model. *ACM Trans. Graph.*, 34(6):248:1–248:16, 2015. [6](#)
- [22] Tiezheng Ma, Yongwei Nie, Chengjiang Long, Qing Zhang, and Guiqing Li. Progressively generating better initial guesses towards next stages for high-quality human motion prediction. In *IEEE/CVF Conference on Computer Vision and Pattern Recognition, CVPR 2022, New Orleans, LA, USA, June 18-24, 2022*, pages 6427–6436, 2022. [2](#), [3](#), [4](#), [6](#), [8](#)
- [23] Naureen Mahmood, Nima Ghorbani, Nikolaus F. Troje, Gerard Pons-Moll, and Michael J. Black. AMASS: archive of

- motion capture as surface shapes. In *2019 IEEE/CVF International Conference on Computer Vision, ICCV 2019, Seoul, Korea (South), October 27 - November 2, 2019*, pages 5441–5450, 2019. 2, 6
- [24] Wei Mao, Miaomiao Liu, and Mathieu Salzmann. History repeats itself: Human motion prediction via motion attention. In *Computer Vision - ECCV 2020 - 16th European Conference, Glasgow, UK, August 23-28, 2020, Proceedings, Part XIV*, pages 474–489, 2020. 1, 3, 4, 5, 6, 7, 12
- [25] Wei Mao, Miaomiao Liu, Mathieu Salzmann, and Hongdong Li. Learning trajectory dependencies for human motion prediction. In *2019 IEEE/CVF International Conference on Computer Vision, ICCV 2019, Seoul, Korea (South), October 27 - November 2, 2019*, pages 9488–9496, 2019. 1, 2, 3, 4, 5, 6, 7, 12
- [26] Wei Mao, Miaomiao Liu, Mathieu Salzmann, and Hongdong Li. Multi-level motion attention for human motion prediction. *Int. J. Comput. Vis.*, 129(9):2513–2535, 2021. 1, 3, 4, 6, 7, 12
- [27] Julieta Martinez, Michael J. Black, and Javier Romero. On human motion prediction using recurrent neural networks. In *2017 IEEE Conference on Computer Vision and Pattern Recognition, CVPR 2017, Honolulu, HI, USA, July 21-26, 2017*, pages 4674–4683, 2017. 1, 3, 6, 12
- [28] Omar Medjaouri and Kevin Desai. HR-STAN: high-resolution spatio-temporal attention network for 3d human motion prediction. In *CVPR Workshops*, pages 2539–2548, 2022. 1, 3
- [29] Vinod Nair and Geoffrey E. Hinton. Rectified linear units improve restricted boltzmann machines. In *Proceedings of the 27th International Conference on Machine Learning (ICML-10), June 21-24, 2010, Haifa, Israel*, pages 807–814, 2010. 4, 11
- [30] Brian Paden, Michal Cáp, Sze Zheng Yong, Dmitry S. Yershov, and Emilio Frazzoli. A survey of motion planning and control techniques for self-driving urban vehicles. *IEEE Trans. Intell. Veh.*, 1(1):33–55, 2016. 1
- [31] Adam Paszke, Sam Gross, Francisco Massa, Adam Lerer, James Bradbury, Gregory Chanan, Trevor Killeen, Zeming Lin, Natalia Gimelshein, Luca Antiga, Alban Desmaison, Andreas Köpf, Edward Yang, Zach DeVito, Martin Raison, Alykhan Tejani, Sasank Chilamkurthy, Benoit Steiner, Lu Fang, Junjie Bai, and Soumith Chintala. Pytorch: An imperative style, high-performance deep learning library. *CoRR*, abs/1912.01703, 2019. 6
- [32] Nitish Srivastava, Geoffrey E. Hinton, Alex Krizhevsky, Ilya Sutskever, and Ruslan Salakhutdinov. Dropout: a simple way to prevent neural networks from overfitting. *J. Mach. Learn. Res.*, 15(1):1929–1958, 2014. 5, 11
- [33] Graham W. Taylor, Geoffrey E. Hinton, and Sam T. Roweis. Modeling human motion using binary latent variables. In Bernhard Schölkopf, John C. Platt, and Thomas Hofmann, editors, *Advances in Neural Information Processing Systems 19, Proceedings of the Twentieth Annual Conference on Neural Information Processing Systems, Vancouver, British Columbia, Canada, December 4-7, 2006*, pages 1345–1352. MIT Press, 2006. 1, 3
- [34] Raquel Urtasun, David J. Fleet, and Pascal Fua. 3d people tracking with gaussian process dynamical models. In *2006 IEEE Computer Society Conference on Computer Vision and Pattern Recognition (CVPR 2006), 17-22 June 2006, New York, NY, USA*, pages 238–245. IEEE Computer Society, 2006. 1
- [35] Timo von Marcard, Roberto Henschel, Michael J. Black, Bodo Rosenhahn, and Gerard Pons-Moll. Recovering accurate 3d human pose in the wild using imus and a moving camera. In *Computer Vision - ECCV 2018 - 15th European Conference, Munich, Germany, September 8-14, 2018, Proceedings, Part X*, pages 614–631, 2018. 2, 6
- [36] Jack M. Wang, David J. Fleet, and Aaron Hertzmann. Gaussian process dynamical models for human motion. *IEEE Trans. Pattern Anal. Mach. Intell.*, 30(2):283–298, 2008. 1, 3

A. Model Implementation Details

We use PyTorch to implement *FreqMRN*.

For the motion attention module, $f_q(\cdot)$ and $f_k(\cdot)$ are implemented as 2-layer CNNs. Specifically, the kernel size of these two layers are set to 6 and 5 respectively with intermediate ReLU [29] activation. These kernel size choices without padding provide us with a receptive field of 10 which corresponds to the query length L .

For the motion refinement module, we iteratively perform $N = 3$ learning stages, each of which contains $K = 5$ GLBs ($M = 2$). Each GLB sequentially executes GC, batch normalization [12], tanh activation and dropout [32]. The dropout ratio is set to 0.3. We set $d = 256$ as the latent representation dimension for both motion attention module and motion refinement module.

Adam [15] is used as the optimizer for all experiments, with 0.005 as the initial learning rate. For Human3.6M dataset, the model is trained for 200 epochs with 32 as the batch size, and the learning rate is multiplied by 0.97 at each epoch. For AMASS and 3DPW datasets, we train the model for 250 epochs with batch size 128, and the learning rate is multiplied by 0.98 at each epoch. *FreqMRN* has around 2.30 million parameters for training on Human3.6M dataset. We use NVIDIA V100 GPUs to train *FreqMRN* for all experiments.

B. More Results for Human3.6M Dataset

In Tab. 7 and Tab. 8, we show a detailed quantitative performance comparison of some representative state-of-the-art methods for short-term and long-term predictions on the Human3.6M dataset. *FreqMRN* outperforms other approaches on most actions and achieves the best average performance.

scenarios	walking				eating				smoking				discussion			
	80ms	160ms	320ms	400ms	80ms	160ms	320ms	400ms	80ms	160ms	320ms	400ms	80ms	160ms	320ms	400ms
millisecons																
Res. Sup. [27]	23.2	40.9	61.0	66.1	16.8	31.5	53.5	61.7	18.9	34.7	57.5	65.4	25.7	47.8	80.0	91.3
convSeq2Seq [18]	17.7	33.5	56.3	63.6	11.0	22.4	40.7	48.4	11.6	22.8	41.3	48.9	17.1	34.5	64.8	77.6
LTD [25]	11.1	21.4	37.3	42.9	7.0	14.8	29.8	37.3	7.5	15.5	30.7	37.5	10.8	24.0	52.7	65.8
HRI [24]	10.0	19.5	34.2	39.8	6.4	14.0	28.7	36.2	7.0	14.9	29.9	36.4	10.2	23.4	52.1	65.4
MMA [26]	9.9	19.3	33.7	39.0	6.2	13.7	28.1	35.3	6.8	14.5	29.0	35.5	9.9	22.8	51.0	64.0
siMLPe [9]	9.9	-	-	39.6	5.9	-	-	36.1	6.5	-	-	36.3	9.4	-	-	64.3
Ours	9.0	17.9	31.6	36.7	5.6	12.7	26.7	33.9	6.2	13.5	28.1	35.1	8.7	21.4	49.7	62.9
scenarios	directions				greeting				phoning				posing			
	80ms	160ms	320ms	400ms	80ms	160ms	320ms	400ms	80ms	160ms	320ms	400ms	80ms	160ms	320ms	400ms
Res. Sup. [27]	21.6	41.3	72.1	84.1	31.2	58.4	96.3	108.8	21.1	38.9	66.0	76.4	29.3	56.1	98.3	114.3
convSeq2Seq [18]	13.5	29.0	57.6	69.7	22.0	45.0	82.0	96.0	13.5	26.6	49.9	59.9	16.9	36.7	75.7	92.9
LTD [25]	8.0	18.8	43.7	54.9	14.8	31.4	65.3	79.7	9.3	19.1	39.8	49.7	10.9	25.1	59.1	75.9
HRI [24]	7.4	18.4	44.5	56.5	13.7	30.1	63.8	78.1	8.6	18.3	39.0	49.2	10.2	24.2	58.5	75.8
MMA [26]	7.2	18.0	43.4	55.0	13.6	29.9	62.9	77.2	8.4	18.0	38.3	48.4	9.8	23.7	57.8	74.9
siMLPe [9]	6.5	-	-	55.8	12.4	-	-	77.3	8.1	-	-	48.6	8.8	-	-	73.8
Ours	6.3	16.8	41.6	52.8	11.6	27.0	58.9	72.8	7.6	16.9	36.8	46.5	8.3	21.6	54.3	70.7
scenarios	purchases				sitting				sitting down				taking photo			
	80ms	160ms	320ms	400ms	80ms	160ms	320ms	400ms	80ms	160ms	320ms	400ms	80ms	160ms	320ms	400ms
Res. Sup. [27]	28.7	52.4	86.9	100.7	23.8	44.7	78.0	91.2	31.7	58.3	96.7	112.0	21.9	41.4	74.0	87.6
convSeq2Seq [18]	20.3	41.8	76.5	89.9	13.5	27.0	52.0	63.1	20.7	40.6	70.4	82.7	12.7	26.0	52.1	63.6
LTD [25]	13.9	30.3	62.2	75.9	9.8	20.5	44.2	55.9	15.6	31.4	59.1	71.7	8.9	18.9	41.0	51.7
HRI [24]	13.0	29.2	60.4	73.9	9.3	20.1	44.3	56.0	14.9	30.7	59.1	72.0	8.3	18.4	40.7	51.5
MMA [26]	12.8	28.7	59.4	72.8	9.1	19.7	43.7	55.4	14.7	30.4	58.4	71.3	8.2	18.1	40.2	51.1
siMLPe [9]	11.7	-	-	72.4	8.6	-	-	55.2	13.6	-	-	70.8	7.8	-	-	50.8
Ours	11.1	26.8	58.2	71.7	8.4	18.8	42.2	53.8	13.5	29.2	57.5	70.4	7.5	17.1	38.6	49.1
scenarios	waiting				walking dog				walking together				average			
	80ms	160ms	320ms	400ms	80ms	160ms	320ms	400ms	80ms	160ms	320ms	400ms	80ms	160ms	320ms	400ms
Res. Sup. [27]	23.8	44.2	75.8	87.7	36.4	64.8	99.1	110.6	20.4	37.1	59.4	67.3	25.0	46.2	77.0	88.3
convSeq2Seq [18]	14.6	29.7	58.1	69.7	27.7	53.6	90.7	103.3	15.3	30.4	53.1	61.2	16.6	33.3	61.4	72.7
LTD [25]	9.2	19.5	43.3	54.4	20.9	40.7	73.6	86.6	9.6	19.4	36.5	44.0	11.2	23.4	47.9	58.9
HRI [24]	8.7	19.2	43.4	54.9	20.1	40.3	73.3	86.3	8.9	18.4	35.1	41.9	10.4	22.6	47.1	58.3
MMA [26]	8.4	18.7	42.5	53.8	19.6	39.5	71.7	84.1	8.5	17.9	34.3	41.1	10.2	22.2	46.3	57.3
siMLPe [9]	7.8	-	-	53.2	18.2	-	-	83.6	8.4	-	-	41.2	9.6	21.7	46.3	57.3
Ours	7.2	17.0	39.6	50.5	17.8	37.9	72.8	87.0	7.7	16.2	31.8	38.5	9.1	20.7	44.5	55.5

Table 7. Short-term prediction on Human3.6M dataset. MPJPE in millimeter at particular frames (80ms, 160ms, 320ms, 400ms) are reported. 256 samples are tested for each action. The best results are highlighted in **bold**.

scenarios	walking				eating				smoking				discussion			
	560ms	720ms	880ms	1000ms	560ms	720ms	880ms	1000ms	560ms	720ms	880ms	1000ms	560ms	720ms	880ms	1000ms
Res. Sup. [27]	71.6	72.5	76.0	79.1	74.9	85.9	93.8	98.0	78.1	88.6	96.6	102.1	109.5	122.0	128.6	131.8
convSeq2Seq [18]	72.2	77.2	80.9	82.3	61.3	72.8	81.8	87.1	60.0	69.4	77.2	81.7	98.1	112.9	123.0	129.3
LTD [25]	53.1	59.9	66.2	70.7	51.1	62.5	72.9	78.6	49.4	59.2	66.9	71.8	88.1	104.5	115.5	121.6
HRI [24]	47.4	52.1	55.5	58.1	50.0	61.4	70.6	75.7	47.6	56.6	64.4	69.5	86.6	102.2	113.2	119.8
MMA [26]	46.2	51.0	54.4	57.1	48.6	59.9	68.9	73.7	46.5	55.5	63.4	68.7	85.2	100.9	111.6	117.5
siMLPe [9]	46.8	-	-	55.7	49.6	-	-	74.5	47.2	-	-	69.3	85.7	-	-	116.3
Ours	44.5	48.9	51.8	54.1	47.2	58.6	67.9	73.1	46.9	56.1	64.1	69.2	84.7	100.6	110.9	117.1
scenarios	directions				greeting				phoning				posing			
	560ms	720ms	880ms	1000ms	560ms	720ms	880ms	1000ms	560ms	720ms	880ms	1000ms	560ms	720ms	880ms	1000ms
Res. Sup. [27]	101.1	114.5	124.5	129.1	126.1	138.8	150.3	153.9	94.0	107.7	119.1	126.4	140.3	159.8	173.2	183.2
convSeq2Seq [18]	86.6	99.8	109.9	115.8	116.9	130.7	142.7	147.3	77.1	92.1	105.5	114.0	122.5	148.8	171.8	187.4
LTD [25]	72.2	86.7	98.5	105.8	103.7	120.6	134.7	140.9	67.8	83.0	96.4	105.1	107.6	136.1	159.5	175.0
HRI [24]	73.9	88.2	100.1	106.5	101.9	118.4	132.7	138.8	67.4	82.9	96.5	105.0	107.6	136.8	161.4	178.2
MMA [26]	72.4	87.4	99.3	105.7	100.5	116.5	130.7	136.7	66.5	82.3	95.8	104.6	105.8	134.1	157.5	172.9
siMLPe [9]	73.1	-	-	106.7	99.8	-	-	137.5	66.3	-	-	103.3	103.4	-	-	168.7
Ours	69.8	84.9	97.2	104.4	97.7	115.9	129.9	136.5	64.6	80.3	94.1	103.3	101.0	128.7	151.3	166.4
scenarios	purchases				sitting				sitting down				taking photo			
	560ms	720ms	880ms	1000ms	560ms	720ms	880ms	1000ms	560ms	720ms	880ms	1000ms	560ms	720ms	880ms	1000ms
Res. Sup. [27]	122.1	137.2	148.0	154.0	113.7	130.5	144.4	152.6	138.8	159.0	176.1	187.4	110.6	128.9	143.7	153.9
convSeq2Seq [18]	111.3	129.1	143.1	151.5	82.4	98.8	112.4	120.7	106.5	125.1	139.8	150.3	84.4	102.4	117.7	128.1
LTD [25]	98.3	115.1	130.1	139.3	76.4	93.1	106.9	115.7	96.2	115.2	130.8	142.2	72.5	90.9	105.9	116.3
HRI [24]	95.6	110.9	125.0	134.2	76.4	93.1	107.0	115.9	97.0	116.1	132.1	143.6	72.1	90.4	105.5	115.9
MMA [26]	94.5	110.2	124.4	133.1	75.8	92.3	106.0	115.0	96.0	115.0	130.7	141.8	71.8	89.9	104.9	115.2
siMLPe [9]	93.8	-	-	132.5	75.4	-	-	114.1	95.7	-	-	142.4	71.0	-	-	112.8
Ours	93.0	109.1	123.8	132.7	74.7	91.5	105.4	114.5	95.1	114.2	130.0	141.6	69.5	87.2	101.4	111.6
scenarios	waiting				walking dog				walking together				average			
	560ms	720ms	880ms	1000ms	560ms	720ms	880ms	1000ms	560ms	720ms	880ms	1000ms	560ms	720ms	880ms	1000ms
Res. Sup. [27]	105.4	117.3	128.1	135.4	128.7	141.1	155.3	164.5	80.2	87.3	92.8	98.2	106.3	119.4	130.0	136.6
convSeq2Seq [18]	87.3	100.3	110.7	117.7	122.4	133.8	151.1	162.4	72.0	77.7	82.9	87.4	90.7	104.7	116.7	124.2
LTD [25]	73.4	88.2	99.8	107.5	109.7	122.8	139.0	150.1	55.7	61.3	66.4	69.8	78.3	93.3	106.0	114.0
HRI [24]	74.5	89.0	100.3	108.2	108.2	120.6	135.9	146.9	52.7	57.8	62.0	64.9	77.3	91.8	104.1	112.1
MMA [26]	72.7	86.9	97.6	105.1	105.1	117.5	131.6	141.4	51.2	56.2	60.3	63.2	75.9	90.4	102.5	110.1
siMLPe [9]	71.6	-	-	104.6	105.6	-	-	141.2	50.8	-	-	61.5	75.7	90.1	101.8	109.4
Ours	69.0	83.8	95.4	103.4	112.0	124.2	137.7	147.5	48.5	53.5	58.5	61.9	74.5	89.2	101.3	109.2

Table 8. Long-term prediction on Human3.6M dataset. MPJPE in millimeter at particular frames (560ms, 720ms, 880ms, 1000ms) are reported. 256 samples are tested for each action. The best results are highlighted in **bold**.